Ion implanted optical waveguides in nonlinear optical organic crystal

Lukas Mutter, Andrea Guarino, Mojca Jazbinšek, Marko Zgonik* and Peter Günter

Nonlinear Optics Laboratory, Institute of Quantum Electronics, ETH Zurich, CH-8093 Zurich, Switzerland

**Permanent address: Dept. of Physics, University of Ljubljana and J. Stefan Institute, Ljubljana, Slovenia*

Max Döbeli

Ion Beam Physics, Paul Scherrer Institute c/o ETH-Zurich, CH-8093 Zurich, Switzerland

lmutter@phys.ethz.ch

Abstract: We report for the first time to our knowledge optical waveguiding in an organic crystalline waveguide produced by ion implantation. Using H^+ ions a refractive index barrier suitable for waveguiding has been realized in the highly nonlinear optical organic crystal 4-N, N-dimethylamino-4'-N'-methyl-stilbazolium tosylate (DAST). The refractive index changes in the waveguiding region as a function of the distance from the surface have been measured. Maximal refractive index changes of up to -0.2 and -0.1 at wavelengths of 633 nm and 810 nm have been realized, respectively. The waveguide refractive index profiles as a function of the ion fluence have been determined. Planar waveguiding has been demonstrated by polishing sharp edges and using conventional end-fire coupling. The measured losses are $\approx$7 dB/cm at 1.57 μm.

OCIS codes: (230.7390) Waveguides, planar; (160.2100) Electro-optical materials; (260.1180) Anisotropic media

References and links

1. Y. Shi, C. Zhang, H. Zhang, J. H. Bechtel, L. R. Dalton, B. H. Robinson, and W. H. Steier, "Low (Sub-1-Volt) Halfwave Voltage Polymeric Electro-optic Modulators Achieved by Controlling Chromophore Shape," Science **288**, 119-122 (2000).
2. F. Pan, G. Knöpfle, Ch. Bosshard, S. Follonier, R. Spreiter, M. S. Wong, and P. Günter, "Electro-optic properties of the organic salt 4-N, N-dimethylamino-4'-N'-methyl-stilbazolium tosylate," Appl. Phys. Lett. **69**, 13-15 (1996).
3. R. Spreiter, Ch. Bosshard, F. Pan, and P. Günter, "High-frequency response and acoustic phonon contribution of the linear electro-optic effect in DAST," Opt. Lett. **22**, 564-566 (1997).
4. L. Mutter, M. Jazbinšek, M. Zgonik, U. Meier, Ch. Bosshard, and P. Günter,"Photobleaching and optical properties of organic crystal 4-N, N-dimethylamino-4'-N'-methyl stilbazolium tosylate," J. Appl. Phys. **94**, 1356-1361 (2003).
5. T. Kaino, B. Cai, and K. Takayama, "Fabrication of DAST Channel Optical Waveguides," Adv. Funct. Mater. **12**, 599-603 (2002).
6. Ph. Dittrich, R. Bartlome, G. Montemezzani, and P. Günter, "Femtosecond laser ablation of DAST," Appl. Surf. Science, **220**, 88-95 (2003).
7. W. Geis, R. Sinta, W. Mowers, S. J. Deneault, M. F. Marchant, K. E. Krohn, S. J. Spector, D. R. Calawa, and T. M. Lyszczarz, "Fabrication of crystalline organic waveguides with an exceptionally large electro-optic coefficient," Appl. Phys. Lett. **84**, 3729-3731 (2004).

#75349 - $15.00 USD Received 25 September 2006; accepted 28 December 2006

8. S. Manetta, M. Ehrensperger, Ch. Bosshard, and P. Günter, "Organic thin film crystal growth for nonlinear optics: present methods and exploratory developments," C. R. Physique, **3**, 449-462, (2002).
9. M. Thakur, J. Xu, A. Bhowmik, and L. Zhou, "Single-pass thin-film electro-optic modulator based on an organic molecular salt," Appl. Phys. Lett. **74**, 635-637 (1999).
10. P. D. Townsend, P. J. Chandler and L. Zhang, *Optical effects of ion implantation*, (Cambridge U. Press, Cambridge,1994).
11. F. Pan, M.S. Wong, Ch. Bosshard, and P. Günter, "Crystal Growth and Characterization of the Organic Salt 4-N, N-Dimethylamino-4'-N'-Methyl-stilbazolium Tosylate (DAST)," Adv. Mater. **8**, 592-595 (1996).
12. D. Fluck, D. H. Jundt, P. Günter, M. Fleuster, and Ch. Buchal, "Modeling of refractive index profiles of He^+ ion-implanted $KNbO_3$ waveguides based on the irradiation parameters," J. Appl. Phys. **74**, 6023-6031 (1993).
13. C. Solcia, D. Fluck, T. Pliska, P. Günter, St. Bauer, M. Fleuster, L. Beckers, and Ch. Buchal, "The refractive index distribution $n_c(z)$ of ion implanted $KNbO_3$ waveguides," Opt. Commun. **120**, 39-46 (1995).
14. P. D. Townsend, "An overview of ion-implanted optical waveguide profiles," Nuc. Instr. and Meth. B**46**, 18-25 (1990).
15. L. Zhang, P. D. Townsend, P. J. Chandler, and J. R. Kulisch, "Ion implanted waveguides in polymethylmethacrylate," J. Appl. Phys. **66**, 4547-4548 (1989).
16. A.Guarino and P. Günter, "Nondestructive method for the characterization of ion-implanted optical waveguides," Optics Letters **30**, 2412-2414 (2005).

1. Introduction

Organic electro-optic materials combine very fast nonlinearities with low dielectric constants which result in larger optical bandwidths of over 100 GHz compared to standard inorganic materials used in telecommunication[1]. The two organic material classes, electro-optic polymers and organic crystals have been intensively studied as integrated optics constituents during the last years. Polymers are potentially cheap and thin film processing is easy, nevertheless they often show thermal and photochemical instabilities and their nonlinearities are generally lower than in the crystalline counterparts. On the other hand, organic crystals have superior nonlinearities, thermal and photochemical stability, but growth of high quality thin films is still a challenging step on the way to develop very large scale integrated (VLSI) photonic devices.

DAST (4-N, N-dimethylamino-4'-N'-methyl stilbazolium tosylate) is a widely investigated organic crystal with large electro-optic coefficients $r_{11} = 77 \pm 8\,\mathrm{pm/V}$ at 800 nm and $r_{11} = 47 \pm 8\,\mathrm{pm/V}$ at 1535 nm combined with a low dielectric constant ($\varepsilon_1 = 5.2$)[2, 3]. Therefore it is an interesting candidate for high speed applications in telecommunications provided that optical waveguiding is achievable.

Many techniques to produce waveguiding structures in DAST have already been proposed, including photobleaching[4, 5], photolithography[5], fs laser ablation[6], graphoepitaxial melt growth[7] and thin film solution growth[8, 9]. However, a fast standard technique allowing for a reliable thickness control of the guiding layer to a few tens of a micrometer, which is a prerequisite for the production of integrated optical structures, has not yet been established.

We decided to employ ion implantation since it is widely used for the production of waveguides in inorganic materials, for which other techniques can not be applied[10]. We present the fabrication of planar optical waveguides in an organic crystal by ion implantation. We show that the process of H^+ and He^+ ion implantation in organic crystals is essentially different from the phenomenon in inorganic crystals or polymers. We demonstrate that the thickness of the guiding layer can be controlled to a few tens of micrometers by H^+ implantation. Furthermore, we present measurements of the refractive index profile and waveguide modes, and finally demonstrate planar waveguiding by end-fire coupling.

2. Ion implantation experiments

The crystals used in our experiments were grown in our laboratory from supersaturated methanol solution by the temperature lowering method[11]. DAST belongs to the monoclinic point group *m*[2]. The crystallographic *b* axis and the dielectric x_2 axis are normal to the mirror

#75349 - $15.00 USD Received 25 September 2006; accepted 28 December 2006

plane, and the dielectric x_1 axis makes an angle of 5.4° to the polar a axis in the symmetry plane[4]. The single crystals were cut approximately perpendicular to the dielectric axes. The typical sample size was around $7\times4\times4\,\mathrm{mm}^3$ with the longest dimension along x_1. In order to use the largest electro-optic coefficient r_{11}, the guided light should be polarized parallel to x_1 and the refractive index n_1 should be altered to ensure confinement. The x_1x_2 surface polished to $\lambda/4$ surface quality was implanted at room temperature with He^+ or H^+ ions. The ion current was kept at about 2 nA and 40 nA for He^+ and H^+ ions, respectively, while the beam was scanned over an area of $9\times9\,\mathrm{mm}^2$ to avoid thermal damage and to ensure homogenous implantation.

In order to get waveguides of small thickness we used the ions with the lowest energy achievable with the 6 MeV EN Van de Graaff tandem accelerator, that is 720 keV He^+ ions and 1 MeV H^+ ions. To avoid channeling along a crystallographic axis, the samples were tilted relative to normal incidence by 10° for He^+ ion implantation. To additionally reduce the implantation depth of H^+ ions the samples were tilted by 60°. This shortens the implantation depth by a factor of 2, having approximately the same effect as reducing the ion energy to 650 keV at normal incidence according to SRIM (The Stopping and Range of Ions in Matter) calculations (www.srim.org).

3. Refractive index profiles of He^+ and H^+ ion implantation

3.1. Model of ion implantation

The penetrating ion is loosing energy on its track in the target material. This energy deposition $G(z) = dE(z)/dz$, which can be calculated with SRIM, has been shown to be responsible for the refractive index change. $G(z)$ is given by two contributions: electronic energy deposition $G_{el}(z) = (dE(z)/dz)_{el}$ due to electronic excitations prevailing at high ion velocities, and nuclear energy deposition $G_n(z) = (dE(z)/dz)_n$ due to collisions with nuclei that occur as the ion is slower at the end of the ion track. The index change induced by ion irradiation can be modeled assuming that the total refractive index change $\Delta n(z)$ is a sum of the changes due to electronic and nuclear energy deposition[12]:

$$\Delta n(z) = \Delta n_{el}(z) + \Delta n_n(z). \tag{1}$$

The phenomenological dependences are given by[12]

$$\Delta n_n(z) = \Delta n_{n,0}\left[1 - \exp\left(-\phi\frac{G_n(\mu z)}{G_{n,0}}\right)^{\gamma_n}\right] \tag{2}$$

$$\Delta n_{el}(z) = \Delta n_{el,0}\left[1 - \exp\left(-\phi\frac{G_{el}(\mu z)}{G_{el,0}}\right)^{\gamma_{el}}\right], \tag{3}$$

where $\Delta n_{n,0}, \Delta n_{el,0}$ are the saturation refractive index changes. Furthermore, $G_{n,0}, G_{el,0}$ represent the saturation energies and γ_n, γ_{el} the exponential factors for the nuclear and electronic energy deposition, respectively, while ϕ is the ion fluence. The parameter μ accounts for the limited accuracy in the prediction of the ion range obtained with SRIM.

3.2. Reflection scan measurement method

After implantation we investigated the optical properties of the samples by measuring the reflection of a wedge polished surface[13]. The refractive index n is related to the intensity reflection coefficient $R = I_R/I_0$ by the Fresnel formula, where I_0 is the incident light intensity and I_R the reflected one. For normal incidence and negligible absorption, n is given by

$$n = \frac{1+\sqrt{R}}{1-\sqrt{R}}. \tag{4}$$

#75349 - $15.00 USD Received 25 September 2006; accepted 28 December 2006

The sample was polished under an angle of 1° as seen in Fig. 1 to increase the spatial resolution of the measurement in z-direction. With a laser beam focused to less than $5\,\mu$m the sample was then scanned in η direction in steps of $5\,\mu$m yielding a depth resolution in z-direction of about $0.1\,\mu$m. In order to probe the refractive index n_1 the incident light was polarized parallel to the dielectric x_1 axis that is normal to the ηz plane. The back reflected light was deflected by a beam splitter and then detected with a photodiode. Signal distortion due to polishing imperfections were reduced by averaging over 22 scans taken at different positions of the sample by translating it normal to the ηz-plane. In addition the back surface of the sample was polished under an angle of 8° to avoid collection of parasitic light (see Fig.1).

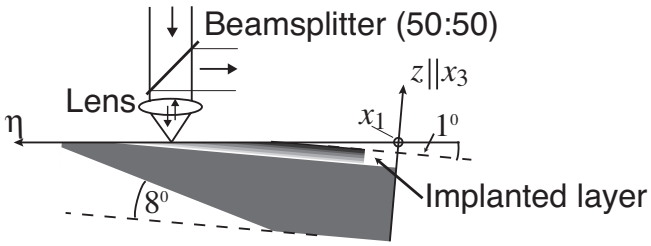

Fig. 1. Experimental setup for the determination of the refractive index profile by measuring the back reflected light from a wedged-polished sample, which was scanned in η direction in steps of $5\,\mu$m yielding a depth resolution of less than $0.1\,\mu$m in z direction.

3.3. *Refractive index profile of He^+ ion implantation*

First implantation experiments were done with 720 keV leading to an ion range of about $3.1\,\mu$m in DAST as shown in Fig. 2. By comparing the magnitude of the electronic and the nuclear

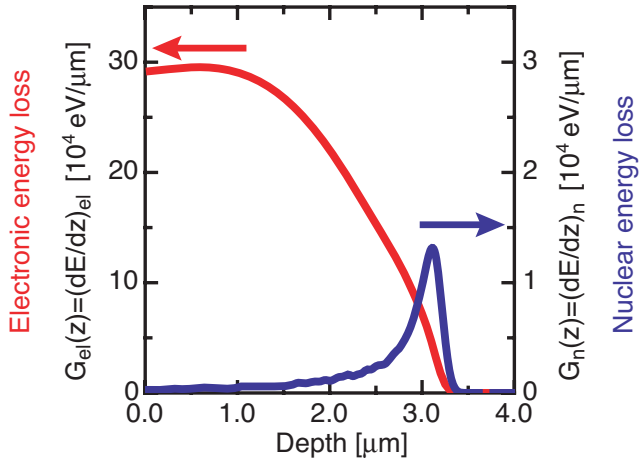

Fig. 2. Nuclear (blue) and electronic (red) energy deposition in dependence on the implantation depth for 720 keV He^+ ions in DAST calculated with SRIM.

energy deposition and the area enclosed by the curves, we see that most of the ion energy is deposited by electronic excitations.

#75349 - $15.00 USD
Received 25 September 2006; accepted 28 December 2006

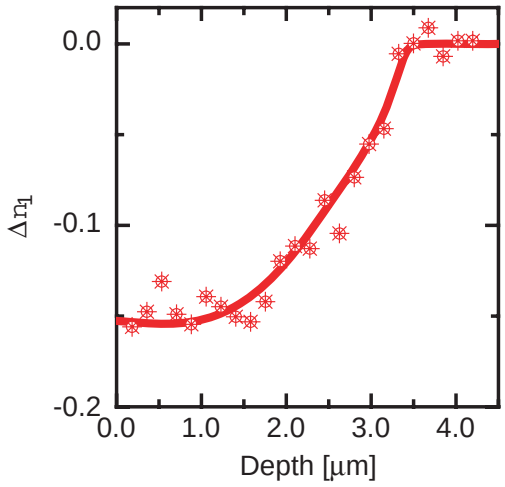

Fig. 3. Refractive index change of n_1 versus implantation depth z at the wavelength 633 nm for 720 keV He^+ ion implantation in DAST with a fluence of $\phi = 0.8 \times 10^{13}$ ions/cm^2 measured with the reflection scan method (Fig.1). The full line is a guide line for the eye.

Implantation with a fluence of 1.5×10^{14} ions/cm^2 of 720 keV He^+ resulted in a large reduction of the refractive index of around $\Delta n_1 \approx -0.9$ for $\lambda = 633$ nm at the surface. With a fluence reduced to 0.8×10^{13} ions/cm^2 a maximal refractive index change Δn_1 of about -0.15 was measured at the surface as depicted in Fig. 3. In inorganic materials, such refractive index changes are only possible with fluences that are more than one order of magnitude higher. The refractive index profile in DAST after He^+ implantation has a shape analogous to the electronic energy loss curve. Therefore, we can conclude that the refractive index is dominantly changed due to electronic energy deposition.

The effect of implantation is therefore essentially different compared to inorganic crystals, for which the nuclear displacements at the end of the ion track are the dominant mechanism of the refractive index change, leading to an optical barrier with reduced refractive index[10, 14]. The effect of implantation is also not the same as in the polymer PMMA[14, 15], where an increase of the refractive index was detected and attributed to an increased absorption. In He^+ implanted DAST the refractive index was decreased. We attribute the lowered refractive index to a decrease of the polarizability of some molecules due to broken bonds.

We can conclude that He^+ ion implantation is not suitable for the production of planar waveguide structures in organic crystals, because of the diffusion-like shape of the refractive index profile and the fact that the refractive index is reduced, resulting in an implanted layer with a lower index than the bulk substrate.

3.4. Refractive index profile of H^+ ion implantation

Since the He^+ experiments with ions showed that a decrease of the refractive index induced by electronic energy deposition in DAST is present, we selected an ion with appropriate electronic energy loss profile to produce a refractive index barrier. The electronic energy deposition curves for He^+ and H^+ ions differ considerably in DAST, as it is evident by comparing Fig. 2 and Fig. 4, respectively. Whereas for He^+ ions it is similar to a diffusion-like profile with a maximum at the sample surface, the electronic deposition curve for H^+ ions has a similar shape as the nuclear energy deposition curve showing a peak at the end of the ion track, which would result

#75349 - $15.00 USD Received 25 September 2006; accepted 28 December 2006

in a refractive index barrier.

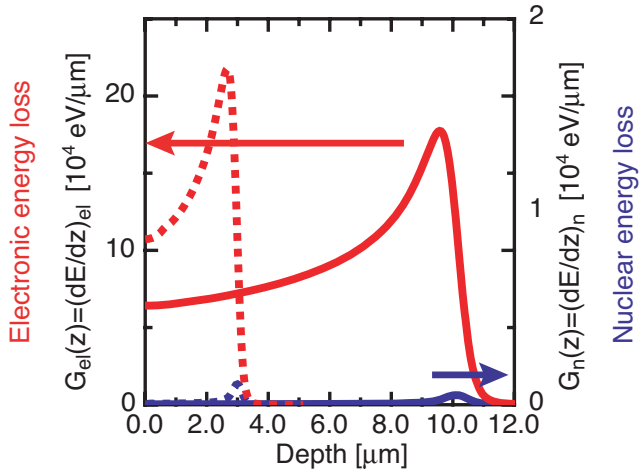

Fig. 4. Nuclear (blue) and electronic (red) energy deposition curve of 450 keV (dashed line) and 1 MeV H^+ ions (full line) in DAST calculated with SRIM. For reason of comparison, ordinate axes with the same order of magnitude as in Fig. 2 have been chosen.

We employed a fluence of 1.25×10^{14} ions/cm^2 to produce a refractive index barrier. The measured profile of the refractive index change Δn_1 is shown in Fig. 5 for wavelengths of 633 nm and 810 nm. Peak refractive index changes of around -0.2 at 633 nm ($n_1 = 2.69$) and -0.1 at 810 nm ($n_1 = 2.36$) were measured. The difference of these values in this small wavelength range can be attributed to the large dispersion of DAST since the wavelength of 633 nm is close to the absorption region. The solid curves in Fig. 5a) and b) are theoretical curves based

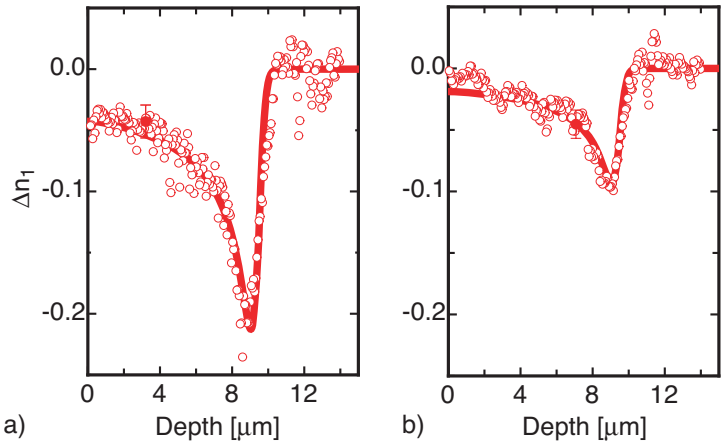

Fig. 5. Refractive index change of n_1 versus implantation depth z at the wavelength 633 nm (a) and 810 nm (b) for 1 MeV H^+ ion implantation in DAST with a fluence of $\phi = 1.25 \times 10^{14}$ ions/cm^2 measured with the reflection scan measurement method. The full lines are theoretical curves based on the theoretical model. The corresponding parameters are summarized in Table1.

#75349 - $15.00 USD
Received 25 September 2006; accepted 28 December 2006

on the model described in section 3.1 with the following remarks. According to the results of He^+ implantation in DAST we can conclude that $\Delta n_{el} \gg \Delta n_n$ and therefore the nuclear contribution to the total index change can be neglected. Since for low fluences far below the saturation level the exponential term of $\Delta n_{el}(z)$ can be linearized, the parameters $\Delta n_{el,0}$ and $G_{el,0}$ cannot be independently modeled. Analysis showed that we are in the low fluence regime and therefore $G_{el,0}$ was fixed to 50×10^{22} eV/cm^3. With this assumption we determined the parameters of Eq.(3) which correspond best to our experimental data. The results are listed in Table 1. In the low fluence regime the exponential factor describes the nonlinear relation between the refractive index change and deposited energy. Therefore, values of γ_{el} above 1 are desirable for the production of optical waveguides in order to have a clear distinction between the barrier region and the guiding layer combined with small refractive index changes in the waveguide core.

Table 1. Model parameters of Eq.(3), which correspond best to the experimental data shown in Fig. 5 obtained by a least square theoretical analysis.

$\Delta n_{el,0}$ @ 633 nm	$\Delta n_{el,0}$ @ 810 nm	$G_{el,0}[10^{22}$eV/cm$^3]$	γ_{el}	μ
0.94±0.05	0.42±0.03	50	1.68±0.05	1.07±0.05

4. Mode analysis

4.1. Barrier coupling method

In order to study the impact of the fluence on the refractive index profile, which is of great importance for a suitable waveguide tailoring, we employed implantations with three different fluences: 1.25×10^{14} ions/cm^2, 1.0×10^{14} ions/cm^2 and 0.5×10^{14} ions/cm^2. The mode profiles were measured with the recently developed barrier coupling method[16], which is more suitable for our organic crystal compared to prism coupling since no prism is required and the modes can be measured in a non contact configuration without applying pressure to the sample. A schematic illustration of the method is shown in Fig.6a). The method is based on frustrated total

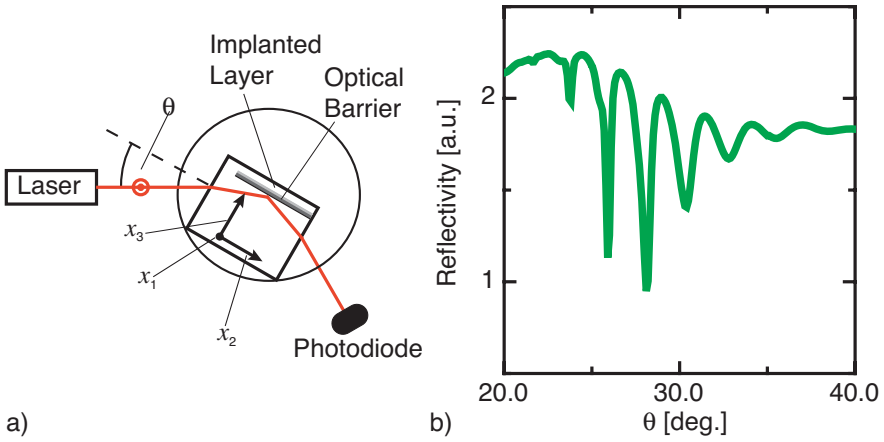

Fig. 6. a) Experimental setup for the determination of the effective mode indices with the barrier coupling method. b) Detected reflectivity as a function of the external angle θ at $\lambda =$ 810 nm for light polarized along the dielectric x_1 axis. The DAST sample was implanted with 1 MeV H^+ ions with a fluence of 1.0×10^{14} ions/cm^2.

#75349 - $15.00 USD Received 25 September 2006; accepted 28 December 2006

internal reflection on the waveguide barrier. The light beam with a vacuum wavenumber k_0 is coupled from the substrate with refractive index n_s to the waveguide core through the optical barrier. If the component of the wave-vector along the waveguide propagation direction x_2 of the beam $\beta = k_0\sqrt{n_s^2 - sin^2(\theta)}$ matches one of the waveguide mode propagation constants $\beta = k_0 \cdot N_{\text{eff}}$, then the evanescent field of the reflected laser light is coupled to a waveguide mode. Coupling results in a dip in the reflection intensity. A measurement of the reflected light as a function of the external incident angle θ for a DAST sample implanted with 1 MeV H^+ ions with a fluence of 1.0×10^{14} ions/cm^2 is shown in Fig. 6b). Eight TE modes for laser light polarized along the dielectric x_1 axis were detected. This measurement confirmed the creation of a waveguide by H^+ ion implantation.

4.2. Results

We compared the effective mode indices measured by the barrier coupling method with those stemming from the refractive index profiles obtained in section 3.4 by the reflection scan method. These were calculated using a 2 × 2 matrix formalism[10]. The refractive index profiles for the three different fluences 1.25×10^{14} ions/cm^2, 1.0×10^{14} ions/cm^2 and 0.5×10^{14} ions/cm^2 obtained with the parameter summarized in Table 1 are shown in Fig. 7a) and the corresponding effective mode indices in Fig.7b). The measured modes (○) and the calculated modes (full line) are in good agreement within the experimental error. The barrier of

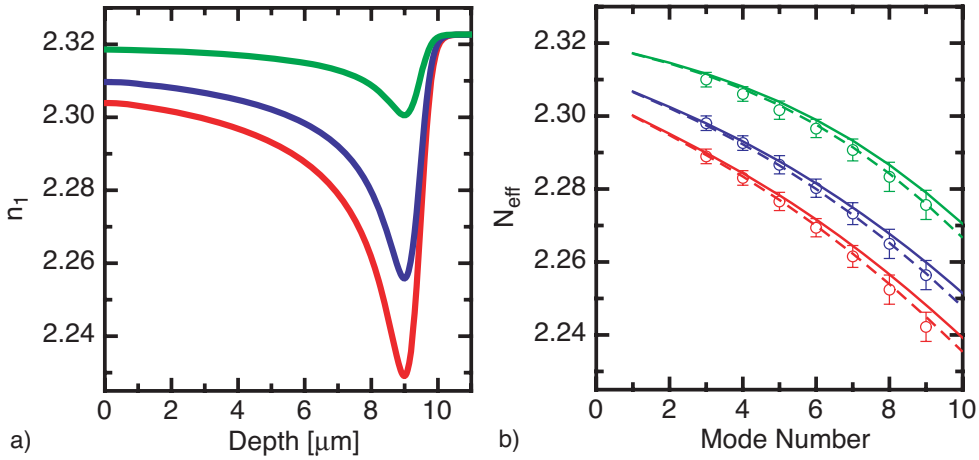

Fig. 7. a) Refractive index profiles at $\lambda = 850$ nm for fluences of 1.25×10^{14} ions/cm^2 (red), 1.0×10^{14} ions/cm^2 (blue) and 0.5×10^{14} ions/cm^2 (green) calculated with the parameters obtained with the reflection scan measurement method. b) Corresponding calculated (full line) and measured (○) effective mode indices N_{eff}; the calculated modes indices are connected for clarity reasons. The dashed lines for the effective indices correspond best to the measured modes obtained by a reduction of the barrier position of about 5% compared to the depicted refractive index profiles in a).

the produced waveguides is thick, which is good to keep the losses low. However, the barrier coupling method cannot be used for modes with low tunneling losses and therefore the first two modes were not detectable as is visible by comparing the measured and calculated modes. Beacuse of limited accuracy in the ion range predicted by SRIM, we varied the barrier position obtained by the reflection scan method ($\mu = 1.07 \pm 0.05$) within the experimental error. The dashed lines shown in Fig. 7a) correspond the best to our experimental data and were ob-

#75349 - $15.00 USD Received 25 September 2006; accepted 28 December 2006

tained by assuming a reduced implantation depth of about 10% ($\mu = 1.11$) compared to SRIM calculations.

5. Waveguiding experiments

After implantation the x_1x_3 end-faces were polished and waveguiding experiments performed by standard end-fire coupling. The light was propagating along the x_2-direction and was polarized parallel to the dielectric x_1 axis, which is the most interesting configuration for optical modulation in DAST in order to use the largest electro-optic coefficient r_{11}. The experimental setup is shown in Fig.8a). Waveguiding was clearly observed at wavelengths of 840 nm,1315 nm and

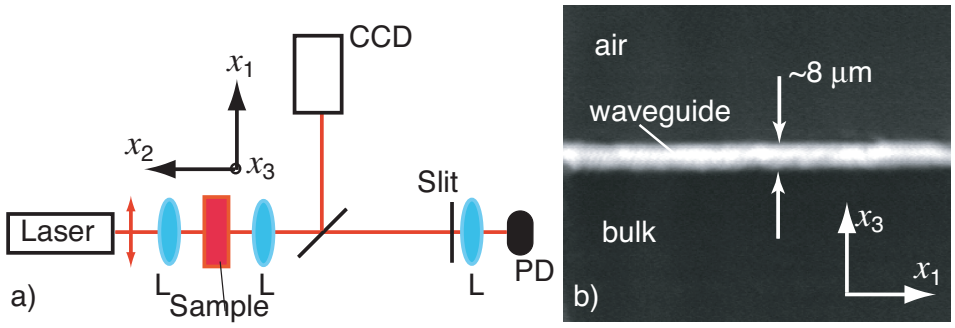

Fig. 8. a) Experimental setup for the determination of the waveguiding characteristics and loss determination: L: lens, CCD: infrared camera, PD: photodiode. b) Photograph of the end-face of the crystal taken with the CCD camera. The cross section of the planar guided light at 1570 nm is clearly visible.

1570 nm. Figure 8b) shows a photograph of the end-face as taken with the infrared camera of the setup with light coupled at 1570 nm.

The losses of the planar waveguide structures were determined by measuring the power of the guided light transmitted through the waveguide with the setup shown in Fig.8 at $\lambda = 1.57\,\mu$m. The guided light was collected with two lenses and detected with a photodiode. Special care was taken to only detect the guided light. Therefore, the polished end face of the crystal sample was imaged onto a horizontal slit that was aligned so that only the guided light could be transmitted. For an assumed coupling efficiency of 80%, the losses were 7 ± 2 dB/cm for the waveguide produced by the ion fluence of 1.0×10^{14} ions/cm^2 and about 10 dB/cm for two other waveguides. The contribution of bulk material absorption is about 2.5 dB/cm at 1.57 μm. At the present state it is not clear if the slightly increased losses for lower 0.5×10^{14} ions/cm^2 and higher 1.25×10^{14} ions/cm^2 fluences are related to higher tunneling losses or defect concentration or to a reduced edge quality and therefore lower coupling efficiency.

6. Conclusions

In conclusion, we have realized optical waveguides in the organic crystal DAST by H^+ ion implantation. Waveguiding with losses of 7 dB/cm at 1.57μm has been achieved in planar waveguides. We have shown that the main refractive index changes in the organic crystal DAST are due to changes in the molecular structure and are caused by the electronic excitations. This result is a new and unexpected finding and completely different from inorganic materials, for which the origins of the refractive index change are ion induced nuclear displacements. Therefore the work gives new perspectives for the use of ion implantation in integrated optics, being

#75349 - $15.00 USD Received 25 September 2006; accepted 28 December 2006

for the first time successfully applied to organic crystals. Refractive index changes in the barrier region of up to -0.1 at 810 nm have been observed at relatively low fluences of the order of 10^{14} ions/cm^2. We have determined the refractive index profile as a function of the H^+ ion fluence by measuring the reflectivity of a wedged-polished sample and confirmed by measuring the effective mode indices by the barrier coupling method. Using these data the effect of ion implantation could be accurately described with a model. Since the waveguide thickness can be tailored by the implantation process within a few tens of micrometers, an important first step towards integrated optics in DAST has been made.

Acknowledgments

We thank J. Hajfler for careful sample preparation and R. Gianotti and M. Sturzeneger for the crystal growth. This work has been supported by the Swiss National Science Foundation.

#75349 - $15.00 USD Received 25 September 2006; accepted 28 December 2006